Biophysical Characterization of the Complex between Double-Stranded RNA and the N-Terminal Domain of the NS1 Protein from Influenza A Virus: Evidence for a Novel RNA-Binding Mode†

Chen-ya Chien,‡ Yujia Xu,§ Rong Xiao,‡ James M. Aramini,‡ Parag V. Sahasrabudhe,‡ Robert M. Krug,|| and Gaetano T. Montelione*,‡,§

Center for Advanced Biotechnology and Medicine and Department of Molecular Biology and Biochemistry, Rutgers University, Piscataway, New Jersey 08854, Department of Biochemistry, Robert Wood Johnson Medical School, University of Medicine and Dentistry of New Jersey, Piscataway, New Jersey 08854, and Institute for Cellular and Molecular Biology, Section of Microbiology and Molecular Genetics, University of Texas at Austin, Austin, Texas 78746

Received July 24, 2003

ABSTRACT: The influenza virus nonstructural protein 1 encoded by influenza A virus (NS1A protein) is a multifunctional protein involved in both protein−protein and protein−RNA interactions. NS1A binds nonspecifically to double-stranded RNA (dsRNA) and to specific protein targets, and regulates several post-transcriptional processes. The N-terminal structural domain corresponding to the first 73 amino acids of the NS1 protein from influenza A/Udorn/72 virus [NS1A(1−73)] possesses all of the dsRNA binding activities of the full-length protein. Both NMR and X-ray crystallography of this domain have demonstrated that it is a symmetric homodimer which forms a six-helix chain fold, a unique structure that differs from that of the predominant class of dsRNA-binding domains, termed dsRBDs, that are found in a large number of eukaryotic and prokaryotic proteins. Here we describe biophysical experiments on complexes containing NS1A(1−73) and a short 16 bp synthetic dsRNA duplex. From sedimentation equilibrium measurements, we determined that the dimeric NS1A(1−73) binds to the dsRNA duplex with a 1:1 stoichiometry, yielding a complex with an apparent dissociation constant (K_d) of ≈1 μM. Circular dichroism and nuclear magnetic resonance (NMR) data demonstrate that the conformations of both NS1A(1−73) and dsRNA in the complex are similar to their free forms, indicating little or no structural change in the protein or RNA upon complex formation. NMR chemical shift perturbation experiments show that the dsRNA-binding epitope of NS1A-(1−73) is associated with helices 2 and 2′. Analytical gel filtration and gel shift studies of the interaction between NS1A(1−73) and different double-stranded nucleic acids indicate that NS1A(1−73) recognizes canonical A-form dsRNA, but does not bind to dsDNA or dsRNA−DNA hybrids, which feature B-type or A/B-type intermediate conformations, respectively. On the basis of these results, we propose a three-dimensional model of the complex in which NS1A(1−73) sits astride the minor groove of A-form RNA with a few amino acids in the helix 2−helix 2′ face forming an electrostatically stabilized interaction with the phosphodiester backbone. This mode of dsRNA binding differs from that observed for any other dsRNA-binding protein.

Influenza virus infection is a major human health problem. In nonpandemic years, influenza infection causes some 20000−30000 deaths per year in the United States alone (*1*). In addition, there are countless losses in both productivity and quality of life for people who overcome mild cases of the disease in just a few days or weeks. Nonstructural protein 1 from influenza A virus (NS1A protein)[1] is required for virus replication (*2*). The NS1A protein is a multi-functional protein that participates in both protein−protein and protein−RNA interactions. Its primary RNA target is double-stranded RNA (dsRNA) (*3*−*5*), and it binds and inhibits the function of two cellular proteins that are required for the 3′-end processing of cellular pre-mRNAs: the 30 kDa subunit of the cleavage and polyadenylation specificity factor (CPSF) and poly(A)-binding protein II (PABII) (*6*−*9*). For these reasons, the NS1A protein is potentially an important target for rational design of antiviral drugs. However, to date no biophysical studies of NS1A in a complex with its dsRNA or specific protein targets have been reported.

† This work was supported by NIH Grants GM-47014 (G.T.M.) and AI 11772 (R.M.K.).

* To whom correspondence should be addressed: CABM-Rutgers University, 679 Hoes Lane, Piscataway, NJ 08854-5638. Phone: (732) 235-5321. Fax: (732) 235-5633. E-mail: guy@cabm.rutgers.edu.

‡ Rutgers University.

§ University of Medicine and Dentistry of New Jersey.

|| University of Texas at Austin.

[1] Abbreviations: 2D, two-dimensional; 3D, three-dimensional; CD, circular dichroism; COSY, correlated spectroscopy; ds, double-stranded; dsRBD, double-stranded RNA-binding domain; dsRNA, double-stranded RNA; EDTA, ethylenediaminetetraacetic acid; FPLC, fast performance liquid chromatography; HSQC, heteronuclear single-quantum coherence; IPTG, isopropyl β-thiogalactopyranoside; NS1A protein, nonstructural protein 1 from influenza A virus; nt, nucleotide; SDS−PAGE, sodium dodecyl sulfate−polyacrylamide gel electrophoresis; ss, single-stranded; TCA, trichloroacetic acid; TOCSY, total correlation spectroscopy.

10.1021/bi030176o CCC: $27.50
Published on Web 01/27/2004

The dsRNA-binding domain of the NS1A protein is located at its amino-terminal end (*10*, *11*). An amino-terminal fragment, which is comprised of the first 73 amino-terminal amino acids [NS1A(1−73)], possesses all the dsRNA binding properties of the full-length protein (*11*). NMR solution and X-ray crystal structures of NS1A(1−73) have shown that in solution it forms a symmetric homodimer with a unique six-helix chain fold (*12*, *13*). Each polypeptide chain of the NS1A(1−73) domain consists of three helices corresponding to residues Asn^{4}−Asp^{24} (helix 1), Pro^{31}−Leu^{50} (helix 2), and Ile^{54}−Lys^{70} (helix 3). Preliminary analysis of NS1A(1−73) surface features suggested two possible nucleic acid binding sites, one involving the solvent-exposed stretches of helices 2 and 2′ comprised largely of basic side chains and the other at the opposite side of the molecule that includes some lysine residues of helices 3 and 3′ (*12*). Subsequent site-directed mutagenesis experiments indicated that the side chains of two basic amino acids (Arg^{38} and Lys^{41}) in the second α-helix are the only amino acid side chains that are required for the dsRNA binding activity of the intact dimeric protein (*14*). These studies also demonstrated that dimerization of the NS1A(1−73) domain is required for dsRNA binding. Replacing Arg^{38} with Lys had no detectable effect on RNA binding, whereas Ala substitution abolished this activity, indicating that a positively charged basic side chain at this position is required for these dsRNA−protein interactions.

These initial studies indicate that the NS1A(1−73) dsRNA-binding domain differs in its mechanism of RNA recognition from the predominant class of dsRNA-binding motifs, termed dsRBDs, that are found in a large number of eukaryotic and prokaryotic proteins (*15*−*19*). Proteins which contain the dsRBD domain include eukaryotic protein kinase R (PKR) (*15*), a kinase that plays a key role in the cellular antiviral response, *Escherichia coli* RNase III (*16*), *Drosophila melanogaster* Staufen (*17*, *18*), and *Xenopus laevis* RNA binding protein A (*19*). Isolated dsRBD domains adopt an α−*β*−*β*−*β*−α topology that folds into a compact structure in which the two α-helices are packed against a three-stranded antiparallel *β*-sheet (*15*−*17*). Structures of dsRBD3 from *D. melanogaster* Staufen and X1rbpa from *X. laevis* in complex with dsRNA (*18*, *19*) revealed the following characteristics of dsRNA binding by dsRBD domains: (i) complex formation does not involve significant structural changes to the protein or the A-form RNA duplex, (ii) protein−RNA interaction is mediated by residues in the α-helices and certain loops, (iii) protein−RNA interactions are consistent with selective but sequence-independent binding to dsRNA, and (iv) the mode of binding in the two cases was not identical.

In this paper, we report the first biophysical studies of NS1A(1−73) in complex with a dsRNA target. These experiments, using a complex of NS1A(1−73) bound to a short synthetic 16 bp dsRNA duplex, identify key features of the mode of protein−RNA interaction. This dsRNA molecule has a sequence derived from a commonly used 29 bp dsRNA-binding substrate which can be generated in small quantities by annealing the sense and antisense transcripts of the polylinker of the pGEM1 plasmid (*11*, *20*). On the basis of sedimentation equilibrium measurements, the stoichiometry of binding of NS1A(1−73) to this synthetic 16 bp dsRNA duplex in solution is 1:1 (one protein dimer with one dsRNA duplex molecule), with a bimolecular dissociation constant (K_d) in the micromolar range. NMR chemical shift perturbation experiments demonstrate that the dsRNA-binding epitope of NS1A(1−73) is associated with antiparallel helices 2 and 2′, as has been previously indicated by site-directed mutagenesis studies (*14*). Circular dichroism (CD) spectra of the purified NS1A(1−73)−dsRNA complex are essentially identical to the sum of CD spectra of free dsRNA and NS1A(1−73), demonstrating that little or no change in the conformations of either the protein or its A-form dsRNA target occurs as a result of binding. Moreover, because we show that NS1A(1−73) binds to neither the corresponding DNA−DNA duplex nor DNA−RNA hybrids, NS1A(1−73) appears to recognize specific conformational features of canonical A-form RNA. Taken together, these results suggest a model in which one dimeric NS1A(1−73) protein binds to one 16 bp dsRNA mediated by electrostatic interactions between the positive side chains in helices 2 and 2′ of the protein and the negatively charged phosphodiester backbone of the dsRNA molecule. This well-characterized, homogeneous 1:1 protein−RNA complex is a suitable reagent for more extensive structural studies.

MATERIALS AND METHODS

Protein Sample Preparation. *E. coli* BL21(DE3) cell cultures were transformed with a pET11a expression vector encoding NS1A(1−73), grown at 37 °C, and then induced with 1 mM IPTG at an OD_{600} of 0.6 for 5 h in MJ minimal medium (*21*) containing uniformly enriched $^{15}NH_4Cl$ and [$^{13}C_6$]glucose as the sole nitrogen and carbon sources, respectively. Cells were broken by sonication, followed by centrifugation at 100000*g* and 4 °C for 1 h. Proteins were then purified from the supernatant by ion exchange and gel filtration chromatography using Pharmacia FPLC systems according to a procedure described previously (*11*). The overall yield of purified NS1A(1−73) was ∼5 mg/L of culture medium. Protein concentrations were determined by the absorbance at 280 nm (A_{280}) using a molar extinction coefficient (ϵ_{280}) for the monomer of 5750 M^{-1} cm^{-1}.

Synthesis and Purification of RNA Oligomers. Two single-stranded (ss) 16-nucleotide RNAs, CCAUCCUCUACAGGCG (sense) and CGCCUGUAGAGGAUGG (antisense), were chemically synthesized using standard phosphoramidite chemistry (*22*) on a model 392 DNA/RNA synthesizer (Applied Biosystems, Inc.). Both RNA oligomers were then desalted over Bio-Rad Econo-Pac 10DG columns and purified by preparative gel electrophoresis on 20% (w/v) acrylamide, 7 M urea denaturing gels. The appropriate product bands, visualized by UV shadowing, were cut out, crushed, and extracted into 90 mM Tris-borate, 2 mM EDTA, pH 8.0 buffer by gentle rocking overnight. The resulting solutions were concentrated by lyophilization and desalted again using Econo-Pac 10DG columns. Purified RNA oligomers were then lyophilized and stored at −20 °C. Analogous 16 nt sense and antisense DNA strands containing the same sequence were purchased from Genosys Biotechnologies, Inc. Concentrations of nucleic acid samples were calculated on the basis of the absorbance at 260 nm (A_{260}) using the following molar extinction coefficients (ϵ_{260}, at 20 °C): 151 530 M^{-1} cm^{-1} for (+) RNA, 165 530 M^{-1} cm^{-1} for (−) RNA, 147 300 M^{-1} cm^{-1} for (+) DNA, 161 440 M^{-1} cm^{-1} for (−) DNA, 262 580 M^{-1} cm^{-1} for dsRNA, 260 060 M^{-1} cm^{-1} for RNA−DNA hybrids, 273 330 M^{-1}

cm^{-1} for DNA−RNA hybrids, and 275 080 M^{-1} cm^{-1} for dsDNA. The extinction coefficients for the single strands were calculated from the extinction coefficients of monomers and dimers at 20 °C (*23*), assuming that the molar absorptivity is a nearest-neighbor property and that the oligonucleotides are single-stranded at 20 °C. Molar extinction coefficients for the duplexes were calculated from the A_{260} values at 20 and 90 °C using the expression $\epsilon_{(260,20°C)} = [A_{(260,20°C)}/A_{(260,90°C)}]\epsilon_{(260,90°C,calc)}$, where $\epsilon_{(260,90°C,calc)}$ is the molar extinction coefficient at 90 °C obtained from the sum of the single strands assuming complete dissociation of the duplex at this temperature.

Polyacrylamide Gel Shift Binding Assay. The single-stranded 16 nt synthetic RNA and DNA oligonucleotides were labeled at their 5′ ends with [γ-^{32}P]ATP using T4 polynucleotide kinase and purified by denaturing urea−PAGE. Approximate 1:1 molar ratios of single-stranded (ss) sense RNA (or DNA) and antisense RNA (or DNA) were mixed in 50 mM Tris, 100 mM NaCl, pH 8.0 buffer. Solutions were heated to 90 °C for 2 min and then slowly cooled to room temperature to anneal the duplexes. NS1A-(1−73), at a final concentration of 0.4 μM, was added to each of the four double-stranded (ds) nucleic acids [dsRNA (RR), RNA−DNA (RD) and DNA−RNA (DR) hybrids, and dsDNA (DD), 10 000 cpm, final concentration of ≈1 nM] in 20 μL of binding buffer [50 mM Tris-glycine, 8% glycerol, 1 mM dithiothreitol, 50 ng/μL tRNA, and 40 units of RNasin (pH 8.8)]. The reaction mixture was incubated on ice for 30 min. The protein−nucleic acid complexes were resolved from free ds or ss oligomers by 15% nondenaturing PAGE at 150 V for 6 h in 50 mM Tris-borate, 1 mM EDTA, pH 8.0 buffer at 4 °C. The gel was then dried and analyzed by autoradiography.

Analytical Gel Filtration Chromatography. Micromolar solutions of the four 16 nt duplexes (RR, RD, DR, and DD) were prepared in 10 mM potassium phosphate, 100 mM KCl, 50 μM EDTA, pH 7.0 buffer and annealed as described above. These duplexes were then purified from unannealed or excess single-stranded species using a Superdex-75 HR 10/30 gel filtration column (Pharmacia), and adjusted to a duplex concentration of 4 μM. Each double-stranded (ds) nucleic acid was then combined with 1.5 mM NS1A(1−73) (monomer concentration) to give a 1:1 molar ratio of protein to duplex. Gel filtration chromatography was performed on a Superdex 75 HR 10/30 column (Pharmacia). This column was calibrated using four standard proteins: albumin (67 kDa), ovalbumin (43 kDa), chymotrypsinogen A (25 kDa), and ribonuclease A (13.7 kDa). Chromatography was carried out in 10 mM potassium phosphate and 100 mM KCl, 50 μM EDTA, pH 7.0 buffer at 20 °C using a flow rate of 0.5 mL/min. Samples of the protein and duplex in a 1:1 molar ratio were applied to the column, and the fractions were monitored for the presence of nucleic acid by their A_{260}; the contribution to the UV absorbance from NS1A(1−73) was ignored because of its relatively small ϵ_{260} compared to the nucleic acid duplexes.

Purification of the NS1A(1−73)−dsRNA Complex. The fraction corresponding to the first peak eluted in the gel filtration chromatography of the 1:1 mixture of the NS1A-(1−73) dimer and dsRNA was collected and concentrated to less than 1 mL using Centricon concentrators (Amicon, Inc.). This sample was then reloaded onto the same gel filtration column, and the main fraction was collected again. The concentration of this purified NS1A(1−73)−dsRNA complex was determined by measuring the UV absorbance at 260 nm. The purity and stability of this complex were also examined using analytical gel filtration by loading 100 μL samples at 5−10 μM immediately following preparation and after 1 month.

Sedimentation Equilibrium. Sedimentation equilibrium experiments were carried out using a Beckman XL-I instrument at 25 °C. Analyses were conducted separately for dimeric NS1A(1−73) and dsRNA, using Beckman eight-channel 12 mm path ("short column") charcoal Epon cells at speeds of 30K−48K rpm, at loading concentrations of 0.2−2 and 0.2−0.6 mg/mL, respectively, to independently evaluate the behavior of these free components. Data were acquired using a Rayleigh interference optical system. To investigate the association behavior of the NS1A(1−73) dimer and dsRNA, analyses were conducted on samples of the complex purified by gel filtration chromatography, using Beckman six-channel 1.2 cm path ("long column") charcoal Epon cells at speeds of 16K−38K rpm. These data were acquired using a UV absorbance optical system at 260 nm and loading concentrations of 0.3, 0.5, and 0.6 absorbance unit. To ensure sample equilibration, measurements were taken every 0.5 h for 4 h for the short column and every 1−6 h for 8−28 h for the long column. Equilibrium was determined to have been established when the difference between two scans taken 1 h apart, calculated using the program WINMACH (developed by D. A. Yphantis and J. Larry, distributed by the National Analytical Ultracentrifugation Facility at The University of Connecticut, Storrs, CT), was within 0.005−0.008 fringe for the Rayleigh interference optics, or ∼0.005 OD_{260} unit for absorbance optics.

Data analysis was performed using program WINNL106, a Windows 95 version based on the original nonlinear least-squares program NONLIN (*24*). The data were fit either separately for each data set at a specific loading concentration and speed or jointly by combining several sets of data with different loading concentrations and/or speeds. The global fit refers to the fitting conducted by using all data sets and with the association constant (ln K) treated as a common parameter. To avoid the complications caused by the deviation from Beer's law, the absorbance data were edited with an OD cutoff value of ≤1.0 from the base region, unless otherwise noted.

The partial specific volume of NS1A(1−73), $\bar{v}_{NS1}$, and the solvent density, ρ, were calculated to be 0.7356 and 1.01156, respectively, at 25 °C using the program Sednterp (*25*). The specific volume of dsRNA, $\bar{v}_{RNA}$, was determined experimentally to be 0.5716 unit by sedimentation equilibrium of dsRNA samples (see Results for details). The specific volume of the NS1A(1−73)−dsRNA complex, $\bar{v}_{complex}$, was calculated to be 0.672 unit assuming a 1:1 stoichiometry, using the method of Cohn and Edsall (*26*).

Calculation of the Dissociation Constant. Our calculation of the dissociation constant of a 1:1 NS1A(1−73)−dsRNA complex is based upon the assumption that there are equal molar amounts of free NS1A(1−73) protein and free dsRNA in the original solution. This assumption is valid if the gel filtration-purified sample of the complex used in these measurements exists in fact in a 1:1 stoichiometry. In this case, the amount of free dsRNA and the amount of free

NS1A(1−73) correspond to the amounts which dissociated from the 1:1 complex. In addition, since the reduced molecular masses (defined below in eq 2) of the NS1A(1−73) dimer and dsRNA differ only by 3%, which is well within our experimental error of 4−7%, the two free macromolecules are treated as the same hydrodynamic species during sedimentation.

The concentration distribution of the *i*th species of an ideal system at sedimentation equilibrium can be expressed as (*24*)

$$C_i(r) = C_i(r')e^{\sigma_i(r^2/2 - r'^2/2)} \quad (1)$$

where $C_i(r)$ is the weight concentration of the *i*th component at a radius r and r' is a reference position inside the solution column. The σ_i in eq 1 is the reduced molecular weight (*27*):

$$\sigma_i = [M_i(I - \bar{v}_i\rho)\omega^2]/(RT) \quad (2)$$

where M_i and $\bar{v}_i$ in eq 2 are the molecular weight and the partial specific volume of the *i*th species, respectively, R is the gas constant, T is the absolute temperature, and ω is the angular velocity. The concentration is normally expressed on a weight concentration scale (milligrams per milliliter); however, in our case, it is more convenient to use the molar concentration m ($m_i = C_i/M_i$).

On the basis of the principle of conservation of mass (*28*), we can write for the dsRNA

$$m^0_{\mathrm{RNA,t}}(r_b^2/2 - r_m^2/2) = \int_{r_b}^{r_m} m(r)_{\mathrm{RNA,free}} e^{\sigma_{\mathrm{RNA}}(r^2/2 - r'^2/2)} r\,dr + \int_{r_b}^{r_m} m(r)_x e^{\sigma_x(r^2/2 - r'^2/2)} r\,dr \quad (3)$$

where m^0 refers to the concentration of the original solution and $m(r)$ refers to the concentration at radius r at sedimentation equilibrium. The subscripts RNA,t, RNA,free, and RNA,x refer to the total amount of dsRNA, free dsRNA, and dsRNA in the NS1A(1−73)−dsRNA complex, respectively; r_m and r_b are radius values at the meniscus and base of the solution column, respectively. To simplify the results to follow, r' is set to be at the position of r_m. Integration of eq 3 then yields

$$m^0_{\mathrm{RNA,t}}(r_b^2/2 - r_m^2/2) = \frac{m(r_b)_{\mathrm{RNA,free}} - m(r')_{\mathrm{RNA,free}}}{\sigma_{\mathrm{RNA}}} + \frac{m(r_b)_{\mathrm{RNA,x}} - m(r')_{\mathrm{RNA,x}}}{\sigma_x} \quad (4)$$

where $m(r_b)_{\mathrm{RNA,free}}$ and $m(r_b)_{\mathrm{RNA,x}}$ are the concentrations of the dsRNA free and in complex with NS1A(1−73), respectively, at the base of the solution column. We can also write the same equation for the NS1A(1−73) protein. Under the condition that m^0_{RNA} equals m^0_{NS1}, we have

$$\frac{m(r')_{\mathrm{RNA,free}}}{\sigma_{\mathrm{RNA}}}\left[\frac{m(r_b)_{\mathrm{RNA,free}}}{m(r')_{\mathrm{RNA,free}}} - 1\right] = \frac{m(r_b)_{\mathrm{NS1,free}}}{\sigma_{\mathrm{NS1}}}\left[\frac{m(r_b)_{\mathrm{NS1,free}}}{m(r')_{\mathrm{NS1,free}}} - 1\right] \quad (5)$$

Making use of the fact that $\sigma_{\mathrm{RNA}} \cong \sigma_{\mathrm{NS1}}$, for this particular protein−RNA complex, we determine from eq 5 that $m(r')_{\mathrm{RNA,free}} = m(r')_{\mathrm{NS1,free}}$ at the reference position, and thus, $m(r)_{\mathrm{RNA,free}} = m(r)_{\mathrm{NS1,free}}$ at any radius r.

Finally, the absorbance at radius r at sedimentation equilibrium can be expressed as

$$A_{260}(r) = E_x m(r')_{\mathrm{RNA}} e^{\sigma_{\mathrm{RNA}}(r^2/2 - r'^2/2)} + (1/E_x)K_a[E_x m(r')_{\mathrm{RNA}} e^{\sigma_{\mathrm{RNA}}(r^2/2 - r'^2/2)}]^2 \quad (6)$$

In eq 6, $E_x = (\epsilon_{\mathrm{RNA}} + \epsilon_{\mathrm{NS1}})l$, where ϵ is the extinction coefficient and l is the optical path length. K_a is the association constant at a molar concentration scale, and can be expressed as a function of m_x and m_{RNA} (eq 7), when $m_{\mathrm{RNA}} = m_{\mathrm{NS1}}$.

$$K_a = \frac{m_x}{{m_{\mathrm{RNA}}}^2} \quad (7)$$

Thus, the association system of NS1A(1−73) and dsRNA is reduced to a simple system of two components during sedimentation. It can be easily fit with an ideal monomer−dimer self-associating model of NONLIN with the fit parameter $K_2 = K_a/E_x$, and the dissociation constant of the NS1A(1−73)−dsRNA complex, K_d, can be calculated from the following equation

$$K_d = \frac{1}{E_x K_2} \quad (8)$$

NMR Spectroscopy. All NMR data were collected at 20 °C on Varian INOVA 500 and 600 NMR spectrometer systems equipped with four channels. The programs VNMR (Varian Associates), NMRCompass (Molecular Simulations, Inc.), and AUTOASSIGN (*29*) were used for data processing and analysis. Proton chemical shifts were referenced to internal 2,2-dimethyl-2-silapentane-5-sulfonic acid; ^{13}C and ^{15}N chemical shifts were referenced indirectly using the respective gyromagnetic ratios: 0.251449530 for the ^{13}C:^{1}H ratio and 0.101329118 for the ^{15}N:^{1}H ratio (*30*).

Sequence Specific Assignments of NS1A(1−73). NMR samples of free [^{13}C,^{15}N]NS1A(1−73) used for assignment were prepared at a dimer protein concentration of 1.0−1.25 mM in 270 μL of 95% H_2O/5% D_2O solutions containing 50 mM ammonium acetate and 1 mM NaN_3 at pH 6.0 in Shigemi susceptibility-matched NMR tubes. Backbone ^{1}H, ^{13}C, ^{15}N, and $^{13}C^{\beta}$ resonance assignments were determined by automated analysis of triple-resonance NMR spectra of ^{13}C- and ^{15}N-enriched proteins using the computer program AUTOASSIGN (*29*). The input for AUTOASSIGN includes peak lists from 2D ^{1}H−^{15}N HSQC and 3D HNCO spectra along with peak lists from three intraresidue [HNCA, CBCANH, and HA(CA)NH] and three interresidue [CA(CO)NH, CBCA(CO)NH, and HA(CA)(CO)NH] experiments. Details of these pulse sequences and optimization parameters are reviewed elsewhere (*31*). Peak lists for AUTOASSIGN were generated by automated peak picking using NMRCompass and then manually edited to remove obvious noise peaks and spectral artifacts. Side chain resonance assignments (except for the ^{13}C assignments of aromatic side chains) were then obtained by manual analysis

of 3D HCC(CO)NH TOCSY, HCCH-COSY, and ^{15}N-edited TOCSY experiments and 2D TOCSY spectra recorded with mixing times of 32, 53, and 75 ms.

NMR Chemical Shift Perturbation Experiments. ^{15}N-enriched NS1A(1−73) was purified and prepared as described above. A 250 μL solution of ^{15}N-enriched NS1A(1−73), 0.1 mM dimer, in 50 mM ammonium acetate, 1 mM NaN_3, and 5% D_2O (pH 6.0) was first used for collecting the $^1H^N-^{15}N$ HSQC spectrum of the free protein. The 16 nt sense and antisense RNA strands in a 1:1 molar ratio were annealed in 200 mM ammonium acetate (pH 7.0), lyophilized three times, and dissolved in the same NMR sample buffer, for a final RNA duplex concentration of 10 mM. This highly concentrated dsRNA solution was then used to titrate the NMR sample of free ^{15}N-enriched NS1A(1−73), making protein−dsRNA samples with ratios of dimeric protein concentration to dsRNA concentration of 2:1, 1:1, 1:1.5, and 1:2. To prevent the precipitation of NS1A(1−73), these samples were prepared by slowly adding the free protein solution to the concentrated dsRNA. The HSQC spectra of free ^{15}N-enriched NS1A(1−73) were acquired with 80 scans per increment and 200 × 2048 complex data points, and transformed into 1024 × 2048 points after zero filling in the t_1 dimension. HSQC spectra for the dsRNA titration experiments were collected with the same digital resolution using 320 scans per increment.

CD Measurements. CD spectra were recorded in the 200−350 nm region at 20 °C using an Aviv model 62-DS spectropolarimeter equipped with a 1 cm path length cell. CD spectra for the four nucleic acid duplexes (RR, RD, DR, and DD) were recorded for 1.1 mL, 5 μM samples in the phosphate buffer described above. Each duplex was then titrated with 1.5 mM NS1A(1−73) (monomer concentration) to form a 1:1 molar ratio of protein to duplex. The CD spectra of these protein−duplex mixtures were recorded under the same conditions; the total duplex concentration remained at 5 μM for each sample. The CD spectra of 1.1 mL samples of free NS1A(1−73) and the column-purified NS1A(1−73)−dsRNA complex, both at 5 μM in the same phosphate buffer, were also acquired. The calculated CD spectra of protein−duplex mixtures were obtained using the sum of CD data from free NS1A(1−73) and from each double-stranded nucleic acid alone. CD spectra are reported as $\epsilon_L - \epsilon_R$, in units of M^{-1} cm^{-1}.

RESULTS

NS1A(1−73) Binds dsRNA but not dsDNA or RNA−DNA Hybrids. NS1A(1−73) and the full-length NS1A protein have been shown to bind double-stranded RNAs (dsRNAs) with no sequence specificity (*4*, *11*, *14*), but it has not been determined if NS1A(1−73) or the NS1A protein binds RNA−DNA hybrids or dsDNA. To test this possibility, we incubated NS1A(1−73) with four ^{32}P-labeled duplexes: 16 bp dsRNA (RR), dsDNA (DD), and two RNA−DNA hybrid duplexes (RD and DR). These mixtures were then analyzed on a native 15% polyacrylamide gel (Figure 1). As reported by others (*32*−*34*), we observe the following migration pattern for the free duplexes on the native gel (fastest to slowest): DD > DR ≈ RD > RR (lanes 1, 3, 5, and 7, respectively). More importantly, only dsRNA was found to form a complex with NS1A(1−73) producing a 30% gel shift

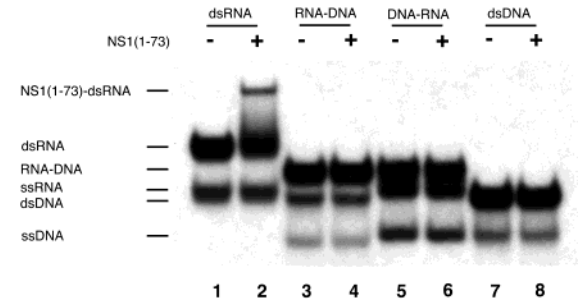

FIGURE 1: Gel shift assay for different duplexes to bind NS1A(1−73). This experiment was performed under standard conditions using indicated ^{32}P-labeled double-stranded nucleic acids (1.0 nM) either with 0.4 μM NS1A(1−73) (+) or without (−).

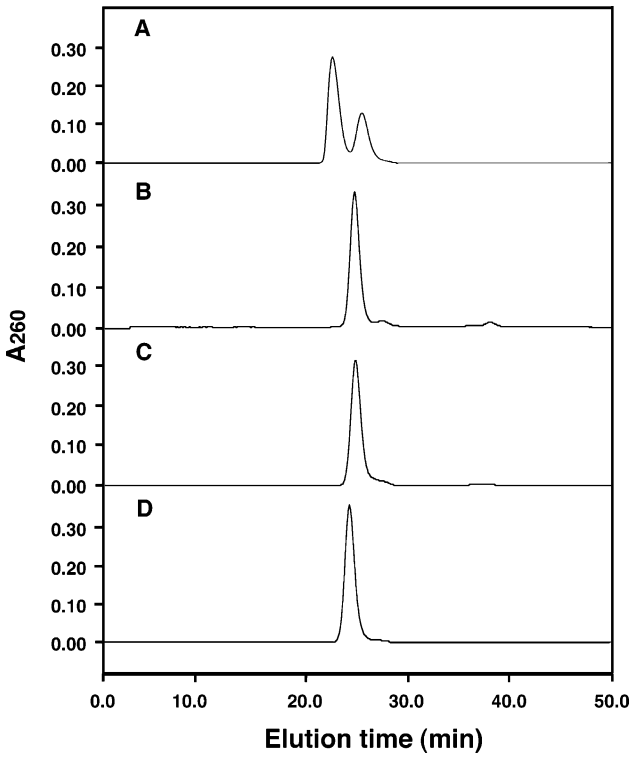

FIGURE 2: Gel filtration chromatography profiles of different duplexes in the presence of NS1A(1−73): (A) dsRNA, (B) RNA−DNA hybrid, (C) DNA−RNA hybrid, and (D) dsDNA. The major peaks between 20 and 30 min correspond to the nucleic acid duplexes, except for the first peak in panel A which is from the NS1A(1−73)−dsRNA complex.

(lane 2), whereas all the other duplexes fail to bind to the protein (lanes 4, 6, and 8). On the basis of these data, we conclude that NS1A(1−73) specifically recognizes conformational and/or structural features of dsRNA (A-form conformation) which are distinct from those of dsDNA (B-form conformation) or RNA−DNA hybrids (intermediate A−B conformations) under these conditions.

Characterization and Purification of the NS1A(1−73)−dsRNA Complex by Gel Filtration Chromatography. The four NS1A(1−73)−nucleic acid duplex mixtures described above were further analyzed for complex formation using analytical gel filtration chromatography. The NS1A(1−73)−dsRNA mixture exhibited two major peaks in the chromatographic profile monitored at 260 nm (Figure 2A), whereas the mixtures containing dsDNA and RNA−DNA hybrids eluted as a single peak (Figure 2B−D). Since the chromatographic eluates were detected by the absorbance at 260 nm, these

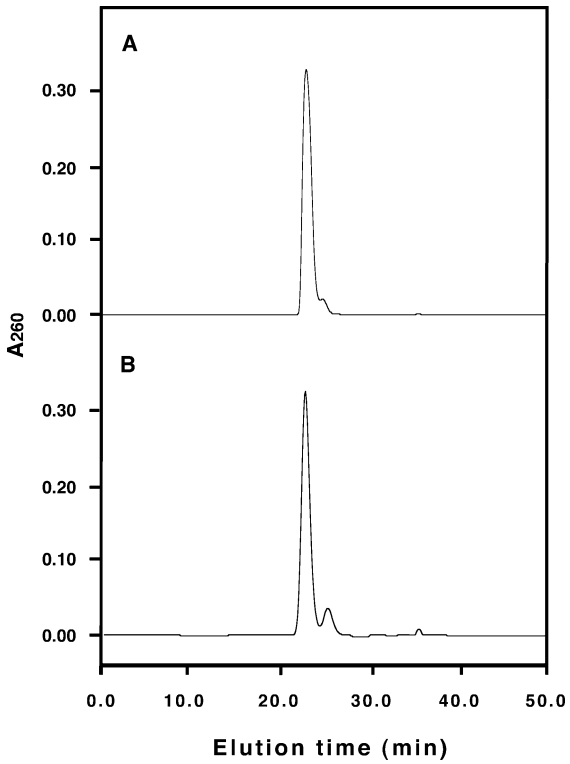

FIGURE 3: Gel filtration chromatograms of the purified NS1A(1−73)−dsRNA complex: (A) 4 μM, with 100 μL of the fresh complex sample, and (B) 4 μM, with 100 μL of the complex sample after 1 month.

chromatograms reflect the state(s) of the nucleic acid in these samples. In the dsRNA case (Figure 2A), the faster and slower eluting peaks correspond to the NS1A(1−73)−dsRNA complex and the unbound dsRNA duplex, respectively. The elution time and corresponding molecular mass (~26 kDa) for the more rapidly eluting peak are consistent with a complex with a 1:1 stoichiometry (protein dimer to dsRNA). Approximately 70% of the RNA and protein are in the complex fraction under the chromatographic conditions that were used. No peak(s) corresponding to complex formation was observed for the other samples. These results confirm that NS1A(1−73) binds exclusively to dsRNA, and not to dsDNA or the RNA−DNA hybrids studied here.

Gel filtration chromatography was also used preparatively to purify the NS1A(1−73)−dsRNA complex prior to subsequent experiments (i.e., sedimentation equilibrium and CD) and to evaluate the long-term stability of the complex (Figure 3). Rechromatographic analysis of the freshly purified NS1A(1−73)−dsRNA complex yielded a single peak consistent with a relatively stable and pure complex (Figure 3A). However, an increase in the amount of free dsRNA was observed after storage at 4 °C for 1 month (Figure 3B), suggesting that the complex slowly and irreversibly dissociates over long periods of time. These results demonstrate that we can use gel filtration chromatography to purify a transiently stable NS1A(1−73)−dsRNA complex, but that this complex slowly dissociates over time.

Sedimentation Equilibrium of Free NS1A(1−73) and dsRNA. We have used sedimentation equilibrium techniques to determine the stoichiometry and dissociation constant of formation of the complex of NS1A(1−73) and the 16 bp dsRNA duplex. First, we conducted short column equilibrium runs on purified NS1A(1−73) protein and purified dsRNA samples with multiple loading concentrations and multiple speeds. The NS1A(1−73) protein exists as a dimer in solution with a molecular mass of 16 851 g/mol, and no obvious signs of dissociation (data not shown). There was evidence, however, of the presence of large, nonspecific aggregates in some of the NS1A(1−73) samples used for these sedimentation experiments. The total amount of aggregate formation varied with each sample and could be separated from the dimer species at high speeds, indicative of a slow sample-dependent aggregation process. Consequently, samples of the protein in complex with dsRNA were purified by gel filtration immediately prior to sedimentation equilibrium measurements (see Figure 3).

The purified dsRNA sample behaved as an ideal solution with a single component during sedimentation. The estimated reduced molecular mass obtained by fitting the data to the single-component model of NONLIN does not change with the loading concentration and/or speed (data not shown). We were, therefore, able to calculate the specific volume of dsRNA from the estimated reduced molecular weight using eq 2 (see Materials and Methods). The value we obtained ($\bar{v}_{RNA}$ = 0.57 cm^3/g) agrees well with the typical partial specific volume values of DNA (0.55−0.59 cm^3/g) and RNA (0.47−0.55 cm^3/g) (*35*). The fact that our value of $\bar{v}_{RNA}$ is closer to that of dsDNA than those of typical RNA samples may be attributed to its double-stranded conformation. A conservative estimate of ~7% error in the reduced molecular weight translates into approximately the same error in the specific volume. In this analysis, it is assumed that the formation of the complex has no significant effect on the specific volume of the dsRNA and the NS1A(1−73) protein.

Stoichiometry and Thermodynamics of Complex Formation Based on Sedimentation Equilibrium. The association of the NS1A(1−73) protein with dsRNA was next studied using samples of the purified NS1A(1−73)−dsRNA complex prepared as described above and validated as being homogeneous by analytical gel filtration (Figure 3A). The stoichiometry of the complex was determined on the basis of data collected at 16 000 rpm (Figure 4A). At this low speed, the free dsRNA and NS1A(1−73) protein have a σ_i value of <0.5 (eq 2). Under these low-speed conditions, the two lower-molecular weight species [i.e., free NS1A(1−73) and free dsRNA] are not significantly redistributed and thus have baseline contributions to the absorbance profile. Accordingly, these data were fit to an ideal single-component model using NONLIN (Figure 4A and Table 1). The estimated apparent molecular masses (M_{app}) of ~24.4 kDa are very close to that of a 1:1 NS1A(1−73)−dsRNA complex calculated from the corresponding amino acid and nucleic acid sequences (27 380 Da). The relatively low rms values and random residual plots (inset of Figure 4A) indicate a good fit to a 1:1 stoichiometry. When the data were edited with an OD_{260} cutoff value of 0.8 from the base of the solution column, the quality of the fit was further improved (Table 1). The estimated average molecular mass of 26 100 g/mol is within ≈3% of the formula molecular mass of a 1:1 NS1A(1−73)−dsRNA complex (27 380 Da). We therefore conclude that this purified NS1A(1−73)−dsRNA complex has a 1:1 stoichiometry.

On the basis of the 1:1 stoichiometry, the data at three different loading concentrations and at three speeds were then fit to the equilibrium monomer−dimer model of NONLIN,

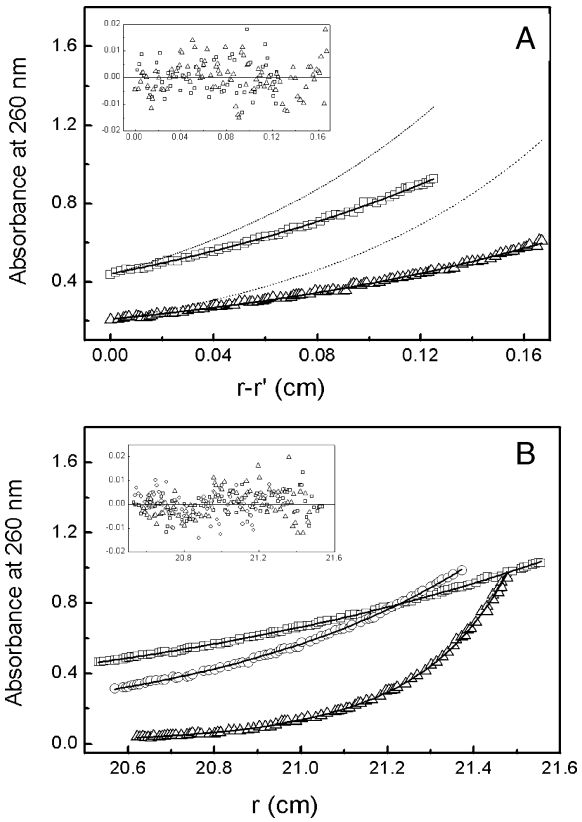

FIGURE 4: (A) Determination of the stoichiometry based on sedimentation equilibrium at 16 000 rpm on three samples with loading concentrations of 0.6 (□), 0.3 (△), and 0.5 (not shown, to avoid the overlap of data points) absorbance unit. The solid line is the joint fit of the three sets of data assuming a 1:1 stoichiometry of the dsRNA−NS1A complex; the inset shows the random residual plots of the fit. The dotted line is drawn assuming a 1:2 stoichiometry of the dsRNA−NS1A complex [the 2:1 complex has a concentration distribution profile nearly identical to those shown by the dotted lines because of the nearly identical reduced molecular mass of dsRNA and NS1A protein (see Materials and Methods)]. (B) Estimation of the dissociation constant from sedimentation equilibrium of three samples (see above) at speeds of 16 000 (□), 22 000 (○), and 38 000 rpm (△). Only the data of the sample with a loading concentration of 0.5 absorbance unit are shown here. The solid lines are the global fit using an ideal monomer−dimer model of NONLIN, and the dissociation constant is calculated from the fitting results using eq 7. The inset shows the residual plots of the fit.

to estimate the dissociation constant, K_d (Figure 4B). Using this model, excellent fits to the data were obtained, as judged by the small rms values and random residual plots. To verify that the fitting model is correct, the individual data sets were also fit separately or jointly using different combinations such as data from a single loading concentration at three different speeds or data from different loading concentrations but at one speed, and so on. For each fit, several different models were compared (data not shown). In all cases, the monomer−dimer model emerges as the best. One exception is the data obtained at 16K rpm which fit equally well to both the single-component system and monomer−dimer models. We also attempted to edit the data with different cutoff values at the base of the cell, and found that the final fitting results were relatively independent of the cutoff between 0.8 and 1.5 absorbance units. The K_d values calculated using eq 8 fall within a relatively narrow range (K_d = 0.4−1.4 μM), depending on the specific fitting that is conducted.

Table 1: Apparent Molecular Mass of the NS1A(1−73)−dsRNA Complex

	NONLIN fitting					
	OD cutoff [b] of ∼1.0			OD cutoff of ∼0.8		
C_t^0 [a]	rms[c]	M_{app}[d]	M_{app}/M_x[e]	rms[c]	M_{app}[d]	M_{app}/M_x[e]
0.6	0.0061	27.5	1.02	0.0051	28.8	1.07
0.5	0.0043	23.3	0.86	0.0040	26.0	0.96
0.3	0.0063	24.9	0.92	0.0065	24.4	0.90
joint fit	0.0056	24.4	0.91	0.0054	25.2	0.94

[a] The concentration of the initial solution measured by absorbance at 260 nm. [b] OD_{260} data greater than the cutoff value were not included in the fit. [c] The root-mean-square value of fitting in units of absorbance. [d] The apparent molecular mass, in kilograms per mole, estimated by fitting the data to an ideal solution with single component (Figure 4A). The data were fit either individually at each loading concentration or jointly for all three data sets together. [e] Ratio of apparent molecular mass (M_{app}) based on sedimentation equilibrium data to the molecular mass of a 1:1 NS1A(1−73)−dsRNA complex calculated from the amino acid and nucleic acid sequence (M_x).

^{1}H, ^{15}N, and ^{13}C Resonance Assignments for Free NS1A-(1−73). Essentially complete NMR resonance assignments for the free NS1A(1−73) protein, required for the analysis of its complex with dsRNA by NMR, have been determined. In all, a total of 65 of 71 (92%) assignable $^{15}N-^1H^N$ sites were assigned automatically using AUTOASSIGN (*29*). This automated analysis provided 71 of 78 H^α, 68 of 73 C^α, 64 of 71 C′, and 44 of 68 C^β resonance assignments via intraresidue and/or sequential connectivities. Subsequent manual analysis of the same triple-resonance data confirmed these results of AUTOASSIGN and also completed the resonance assignments for the remaining backbone atoms and 60 of 68 C^β atoms. All backbone resonances were assigned except Met^1 NH_2, Pro^{31} N, and C′ of C-terminal residue Ser^{73} and Pro-preceding residue Ala^{30}. Complete side chain assignments of nonexchangeable protons and protonated carbons (the aromatic carbons are not included) were then obtained for all residues. With regard to exchangeable side chain groups, all Arg $N^\epsilon H$, Gln $N^{\epsilon 2}H$, Asn $N^{\delta 2}H$, and Trp $N^{\epsilon 1}H$ resonances were also assigned, but no Arg $N^\eta H$ or hydroxyl protons of Ser and Thr were observed in these spectra. These ^{1}H, ^{13}C, and ^{15}N chemical shift data for NS1A-(1−73) at pH 6.0 and 20 °C have been deposited in BioMagResBank (accession number 4317).

The $^1H-^{15}N$ HSQC spectrum for ^{15}N-enriched NS1A(1−73) at pH 6.0 and 20 °C is shown in Figure 5A. All backbone amide peaks (except for Pro^{31} and the N-terminal Met^1) are labeled, as are the side chain resonances of Arg $N^\epsilon H$, Gln $N^{\epsilon 2}H$, Asn $N^{\delta 2}H$, and Trp $N^{\epsilon 1}H$. Overall, the spectrum displays reasonably good chemical shift dispersion, although there are a few degenerate $^{15}N-^1H^N$ cross-peaks. For example, residues Arg^{37} and Arg^{38} have almost the same chemical shifts for H^N, N, C′, C^α, H^α, and C^β resonances.

Epitope Mapping by Chemical Shift Perturbation. In an effort to shed light on the local perturbations to the protein due to dsRNA binding, we monitored the titration of ^{15}N-enriched NS1A(1−73) with the 16 bp dsRNA by collecting a series of $^1H^N-^{15}N$ HSQC spectra. The chemical shifts of both ^{1}H and ^{15}N nuclei are sensitive to their local electronic environment and therefore can be used as probes for interactions between the labeled protein and unlabeled RNA. Presumably, the strongest perturbation of the electronic environment will be observed for the residues that either

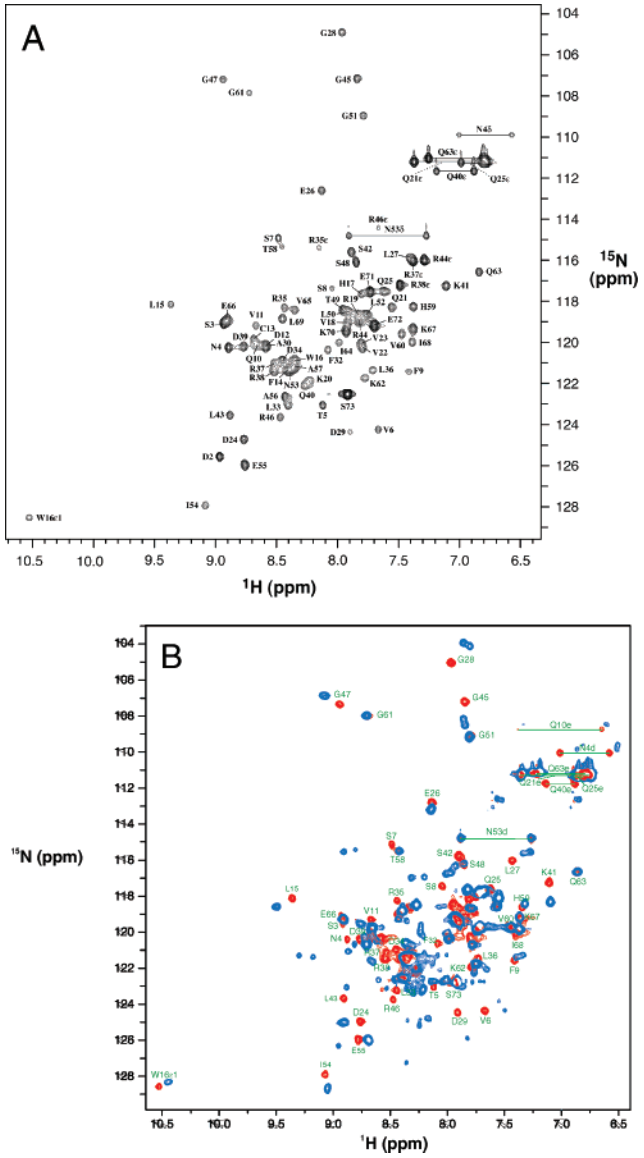

FIGURE 5: (A) Two-dimensional ^{1}H−^{15}N HSQC spectrum of 2.0 mM uniformly ^{15}N-enriched NS1A(1−73) at 20 °C and pH 6.0 in a 95% H_2O/5% D_2O mixture containing 50 mM ammonium acetate and 1 mM sodium azide. The cross-peaks are labeled with respective resonance assignments indicated by the one-letter code of amino acids and a sequence number. Also shown are the side chain NH resonance of the tryptophan and side chain NH_2 resonances for glutamines and asparagines. The peaks assigned to N^{ϵ}−H^{ϵ} resonances of arginines are folded in the F1 (^{15}N) dimension from their positions further upfield. (B) An overlay of represented $^{1}H^{N}$−^{15}N HSQC spectra for ^{15}N-enriched NS1A(1−73) uncomplexed (red) and complexed (blue) with 16 bp dsRNA at pH 6.0 and 20 °C. Labels correspond to amide backbone assignments of well-resolved cross-peaks of the free protein.

come into direct contact with RNA or are involved in major conformational changes upon binding to RNA.

Four HSQC spectra were recorded on samples containing an NS1A(1−73) dimer concentration of 0.1 mM with decreasing molar ratios of dimeric protein to dsRNA of 2:1, 1:1, 1:1.5, and 1:2. Protein was induced to precipitate when this ratio reached above 5:1. In the HSQC spectrum of the 2:1 ratio sample, $^{1}H^{N}$−^{15}N cross-peaks are very broad and difficult to analyze, suggesting that the protein may form higher-molecular mass complexes with dsRNA. The spectra with ≤1:1 stoichiometry exhibited only one set of peaks, despite the improvement in sensitivity when more dsRNA was introduced.

Because of the large size of the NS1A(1−73)−dsRNA complex, *de novo* backbone assignments for NS1A(1−73) in the complex have not been completed to date. However, by comparison of HSQC spectra for free and dsRNA-bound NS1A(1−73) (Figure 5B and data not shown generated in the titration experiments described above), it was observed that while no backbone−amide chemical shifts in helices 3 and 3′ are affected by complex formation, almost all residues in helices 2 and 2′ exhibit ^{15}N and ^{1}H shift perturbations upon complex formation. In addition, several residues in helices 1 and 1′ also exhibit chemical shift perturbations upon complex formation. Changes in ^{15}N and ^{1}H chemical shifts upon binding are mapped onto the three-dimensional structure of free NS1A(1−73) in Figure 6. All of the significant chemical shift perturbations observed upon complex formation (represented in cyan) correspond to NS1A(1−73) backbone atoms that are either in helices 2 and 2′, which contain numerous arginines and lysines, or in helices 1 and 1′, which have close contact with helices 2 and 2′ (Figure 6B). However, residues whose backbone NH groups do not undergo significant chemical shift change, indicative of little or no structural alteration (represented in pink), tend to be distant from the apparent binding epitope. These results confirm our previous identification of the dsRNA binding epitope in regions in or around antiparallel helices 2 and 2′, as indicated previously by site-directed mutagenesis studies (*14*), and further indicate that, as the chemical shifts of amides distant from the binding epitope are not perturbed by complex formation, the overall structure of NS1(1−73) is not altered by dsRNA binding.

Circular Dichroism (CD) Spectroscopy. Circular dichroism provides a useful probe of the secondary structural elements and global conformational properties of nucleic acids and proteins. For proteins, the 180−240 nm region of the CD spectrum mainly reflects backbone conformation (*36*). Changes in the CD spectrum observed above 250 nm upon formation of protein−nucleic acid complexes arise primarily from changes in the nucleic acid secondary structure (*37*). The CD profiles of the four 16 bp duplexes (RR, RD, DR, and DD) are distinct and characteristic of their respective duplex types (Figure 7, red traces) (*38*−*43*). The RR duplex features a slight negative band at 295 nm, a strong negative band at 210 nm, and a positive band near 260 nm, characteristic of the A-form dsRNA conformation (Figure 7A) (*42*−*43*). The DD duplex has roughly equal positive and negative bands above 220 nm, with a crossover resulting in a positive band at 260 nm typical of B-DNA (Figure 7D) (*41*−*43*). The two hybrids, RD and DR, exhibit traits that make them distinct from each other, yet both are roughly intermediate between A-form dsRNA and B-form dsDNA structures (Figure 7B,C) (*32*−*34*, *42*, *43*). In addition, the intensity of the positive band at 260 nm appears to be most sensitive to the A-like character of the hybrid duplex (*43*).

CD spectra of NS1A(1−73) in the presence of an equimolar amount of RR, RD, DR, or DD duplex are shown in Figure 7 (yellow traces). In the dsRNA case (Figure 7A), the gel filtration-purified NS1A(1−73)−dsRNA complex was used to avoid interference due to the presence of free dsRNA (see Figures 2 and 3). In each case, the spectrum of free NS1A(1−73) is also shown (blue traces). NS1A(1−

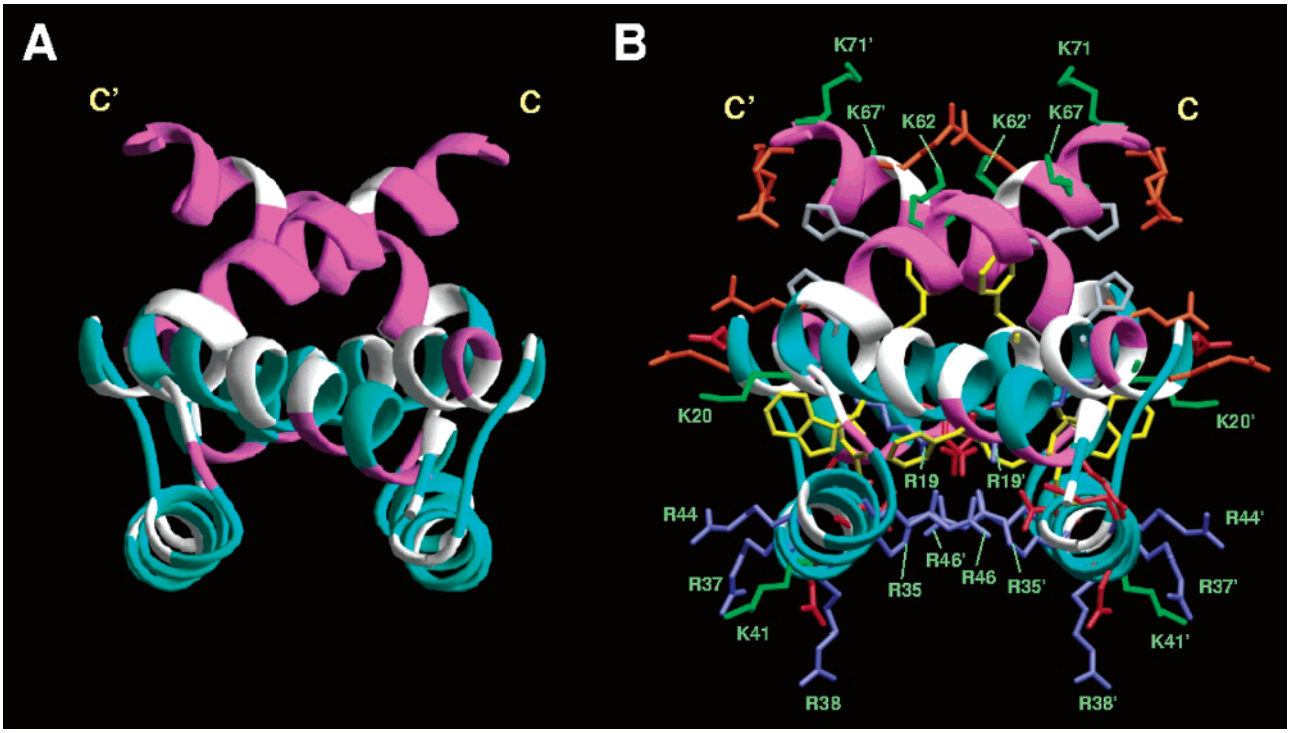

FIGURE 6: (A) Ribbon diagram of NS1A(1−73) showing the results of chemical shift perturbation measurements. Residues of NS1A(1−73) which give shift perturbations in NMR spectra of the NS1(1−73)−dsRNA complex are colored cyan; residues that are not changed in the chemical shifts of their amide ^{15}N and ^{1}H resonances are colored pink, and white represents the chemical shift assignments of the residues that cannot be identified in 2D HSQC spectra due to overlapping cross-peaks. (B) Same ribbon diagram with key side chains displayed. All the basic residues are labeled. Note that the binding epitope of NS1A(1−73) to dsRNA appears to be on the bottom of this structure.

73) backbone amide bands dominate the CD spectra in the 200−240 nm range, while structural information for the nucleic acid duplexes dominates the 250−320 nm region. On the basis of gel shift assay and gel filtration data described above, we have established that only the dsRNA substrate forms a complex with NS1A(1−73). However, as shown in Figure 7A, complex formation (yellow trace) does not result in significant changes to the 250−320 nm region of the CD spectrum that is most sensitive to nucleic acid duplex conformation. Furthermore, the CD spectrum of the dsRNA−NS1A(1−73) complex (yellow) and a spectrum computed by simply adding the spectra of free NS1A(1−73) and free dsRNA (green) are essentially identical in the 200−240 nm region, indicating the NS1A(1−73) backbone structure is also not extensively altered by complex formation. Although NS1A(1−73) does not to bind the other duplexes, the CD spectra for each RD, DR, and DD mixed with an equimolar amount of NS1A(1−73) were obtained as controls (Figure 7B−D). These data confirm that the detected CD spectra of these mixtures are equal to the sum of separate duplex and protein spectra when the structures of these molecules are not changed. Overall, these CD data demonstrate that the RNA duplex retains its A-form conformation in the dsRNA−NS1A(1−73) complex.

DISCUSSION

Using a variety of biophysical techniques, we have assessed the interaction of the N-terminal domain of the NS1 protein from influenza A virus with a 16 bp dsRNA formed from two synthetic oligonucleotides. Our results establish the following: (i) NS1A(1−73) binds to dsRNA, but not to dsDNA or the corresponding hetero duplexes, (ii) this NS1A-(1−73)−dsRNA complex exhibits 1:1 stoichiometry and a dissociation constant of ∼1 μM, (iii) symmetry-related antiparallel helices 2 and 2′ of NS1A(1−73) play a central role in binding the dsRNA target, and (iv) the backbone structures of dsRNA and NS1A(1−73) are not significantly different in the complex and in the corresponding unbound molecules. Overall, this study provides important biophysical evidence for a working hypothetical model of the complex between this novel dsRNA binding motif and duplex RNA. In addition, this study establishes that the complex of NS1A-(1−73) and the 16 bp dsRNA is a suitable reagent for future three-dimensional structural analysis, namely, that it is a homogeneous 1:1 complex.

Biophysical Characterization of the NS1A(1−73)−dsRNA Complex. A wide body of spectroscopic evidence in the literature, including NMR, X-ray, CD, and Raman spectroscopic studies, has established that dsDNA is characterized by a B-type conformation with C2′-endo sugar puckering, dsRNA adopts an A-form structure featuring C3′-endo sugars, and DNA−RNA hybrids exhibit an intermediate conformation between the A- and B-motifs (see, for example, refs *44*−*48*). In addition, the surface features of canonical duplexes differ, with the A-form featuring a wide, shallow minor groove and the B-form being characterized by a narrow, deep major groove. Since NS1A(1−73) clearly binds only to dsRNA, yet without sequence specificity, it is reasonable to conclude that this protein discriminates between these nucleic acid helices largely on the basis of duplex conformation (i.e., A-form conformation). However, the possibility that the molecular recognition process also depends on the presence of 2′-OH groups on each strand of the duplex cannot be ruled out.

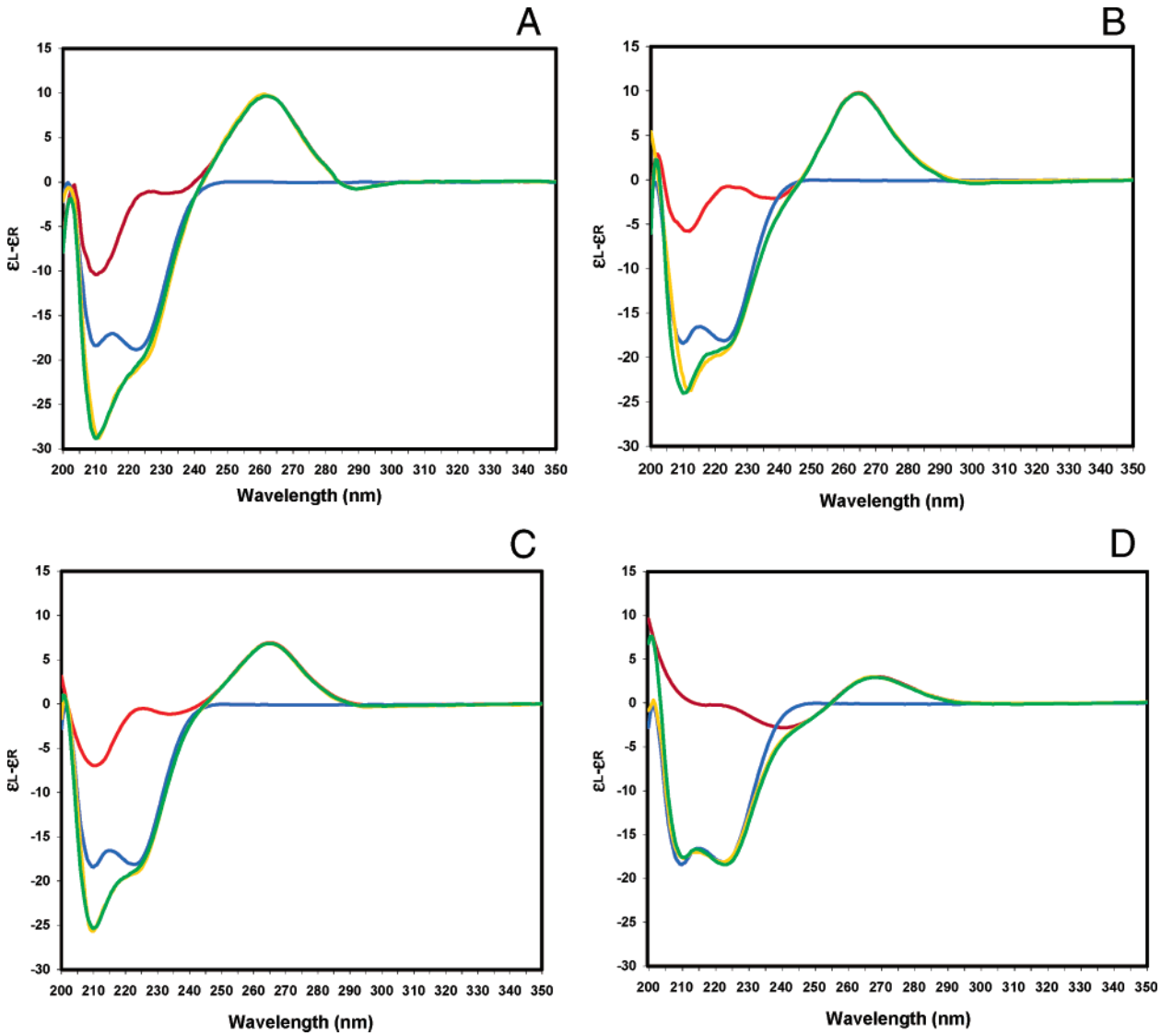

FIGURE 7: CD spectra of the purified NS1A(1−73)−dsRNA complex (A) and the mixtures of duplexes and NS1(1−73): RNA−DNA hybrid (B), DNA−RNA hybrid (C), and dsDNA (D): yellow for the experimental CD spectra of the mixtures (1:1 molar ratio of duplex and protein dimer), red for the duplex alone, blue for NS1A(1−73) alone, and green for the calculated sum spectra of the duplex and NS1A(1−73).

Our results provide an explanation for the binding of the full-length NS1A protein and NS1A(1−73) to another RNA target, a specific stem bulge in one of the spliceosomal small nuclear RNAs, U6 snRNA (*20*). On the basis of the studies of the structural specificity of complex formation described in this paper, we postulate that this stem bulge of U6 snRNA forms an A-form structure like dsRNA in solution, allowing NS1A(1−73) to form a complex with U6 snRNA similar to that characterized in this work between NS1A(1−73) and the 16 bp dsRNA fragment.

On the basis of sedimentation equilibrium experiments, we have established that the NS1A(1−73) dimer binds the dsRNA duplex in a 1:1 fashion with a dissociation constant, K_d, of ∼1 μM. Interestingly, ∼30% of the dsRNA is uncomplexed in size exclusion experiments on 1:1 molar ratios of dimer to duplex (Figure 2A), and even more free dsRNA is detected in the gel shift assays (Figure 1). The fraction of unbound dsRNA was found to vary from one NS1A(1−73) preparation to another, and was not observed in gel filtration chromatograms of freshly purified samples of the complex (Figure 3A). Moreover, we also observed that complexes slowly dissociate during prolonged storage (Figure 3B). Therefore, it appears that NS1A(1−73) exhibits slow irreversible self-aggregation under the conditions used in our studies. This conclusion is also supported by the observation of larger molecules (aggregates) in the sedimentation equilibrium experiments when using laser light scattering as the method of detection.

We emphasize that when the purified NS1A(1−73)−dsRNA complex was reloaded to the gel filtration column, no excessive free dsRNA was observed. The sample behaved like a tight complex with a K_d in the micromolar range, consistent with the estimation from sedimentation equilibrium experiments. Accordingly, complex formation and purification by gel filtration provide a mechanism for isolating the active NS1A(1−73) dimer−active dsRNA complex from "inactive material" present in the sample. Therefore, regardless of the nature of the contaminants, aggregates, and/or incompetent species, no such factors should affect our estimations of the stoichiometry and the dissociation constant based on sedimentation equilibrium experiments using the purified NS1A(1−73)−dsRNA complex. Further, our dem-

onstration that the gel-purified complexes behave as tight, homogeneous complexes indicates that these complexes should be amenable to structural analysis by X-ray crystallography or NMR.

Comparison with Alternate Estimates of the Affinity and Stoichiometry of the NS1A(1−73)−dsRNA Complex. Previous estimates of affinities of the NS1A(1−73)−dsRNA complex using gel shift measurements have produced values of apparent dissociation constants (K_d) ranging from 20 to 200 nM (*14*). These studies were all carried out with small quantities of longer dsRNA substrates that have sequences different from that of the substrate used in the biophysical measurements described above. In this earlier work, it was observed that the stoichiometry of NS1A(1−73)−dsRNA binding (based on the size of gel shifts) depends on the length of the dsRNA substrate, and that the binding is semicooperative (*14*). Similar semicooperative binding results have been reported for full-length NS1A (*4*).

The complex between NS1A(1−73) and a 16 bp dsRNA duplex molecule described in this biophysical study is a model of part of the complete set of interactions that occur when multiple NS1A RNA-binding domains bind along a longer length of dsRNA, as is thought to occur *in vivo*. The 1:1 stoichiometry observed in this model system precludes the possible protein−protein interactions and other cooperative effects which can occur in a multiple-binding mode of a larger system. In the binding of the NS1A protein to larger dsRNAs, the apparent affinity can also be modulated by configurational entropy effects when there are many possible sites for nonspecific binding. For example, Wang *et al*. (*14*) have reported that NS1A(1−73) has a 10-fold higher affinity for a 140 bp dsRNA substrate than for a similar 55 bp dsRNA substrate. For these several reasons, the affinity constant reported here for the simple 1:1 complex of the NS1A(1−73) dimer with a 16 bp segment of dsRNA is lower than the apparent affinities reported previously for larger cooperative systems. However, while the model complex described in this work captures only part of the full structural information for the complete multiple-binding cooperative system, the complex described in this work is well-characterized, easily generated, and more suitable for detailed structural studies of the protein−dsRNA interactions underlying the NS1A−RNA molecular recognition process.

RNA-Binding Site of NS1A(1−73). Alanine scanning mutagenesis studies on NS1A(1−73) (*14*) revealed that in binding to larger dsRNA fragments as well as U6 snRNA (i) the protein must be a dimer to bind its target and (ii) only R38 is absolutely required for RNA binding, though K41 also plays a significant role. The RNA-binding epitope of NS1A(1−73) identified by chemical shift perturbation of $^{15}N-^{1}H$ HSQC resonances described in this paper supports and extends these mutagenesis data. The chemical shifts of practically all of the backbone amide resonances within helices 2 and 2′ are altered upon binding to the dsRNA. This is consistent with a model in which one or more of the solvent-exposed basic side chains of the residues in helices 2 and 2′, including Arg^{38} and Lys^{41} (Figure 6B), are involved in the direct contact with dsRNA. It is also possible that the solvent-exposed basic side chains of Arg^{37} and Arg^{44}, as well as the partially buried side chains of Arg^{35} and Arg^{46} [which participate in intra- and intermolecular salt bridges (*12*, *13*)], also interact with dsRNA directly. Moreover, the chemical shift perturbation data also rule out the involvement of the proposed potential RNA binding site on helices 3 and 3′ (*12*), since most of the backbone $^{1}H^{N}$ and ^{15}N atoms of residues on the third helix do not show any change in chemical shift upon complex formation, indicating that the binding epitope is distant from helices 3 and 3′ and that the overall backbone conformation of NS1A(1−73) is not affected by RNA binding. Chemical shift differences for some residues on helices 1 and 1′ in the protein core region can be ascribed to the local environment changes induced by the RNA interaction. Overall, these NMR data indicate that the six-helix chain fold conformation of NS1A(1−73) remains intact when it binds to dsRNA. This conclusion is completely consistent with the conclusion from CD studies that neither NS1A(1−73) nor dsRNA exhibits extensive backbone structural changes upon complex formation.

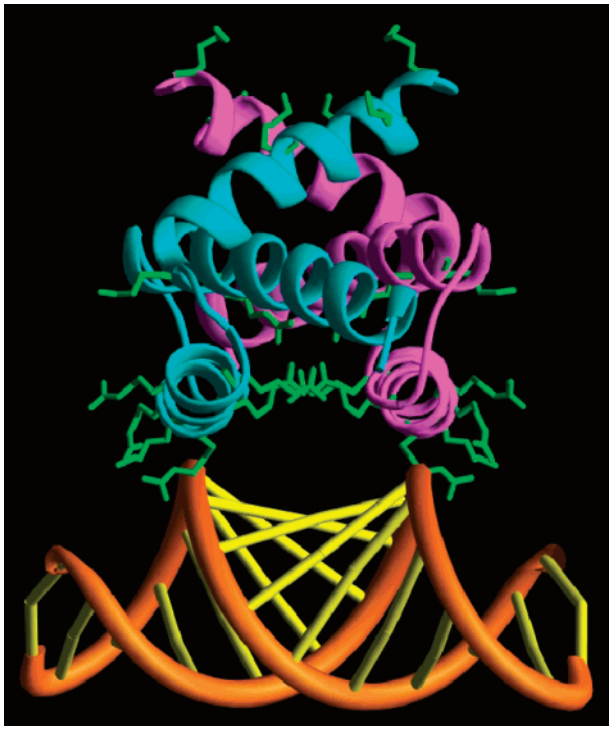

FIGURE 8: *Hypothetical model* that is consistent with our cumulative knowledge of the dsRNA binding properties of NS1A(1−73). *We emphasize that this picture is just a working model, consistent with the available data but useful only for the purpose of designing experiments to test the implied hyoptheses.* Phosphate backbones and base pairs of dsRNA are shown in orange and yellow, respectively. All side chains of Arg and Lys residues are labeled in green. Atomic coordinates for this model are available from the authors (guy@cabm.rutgers.edu).

A 3D Model of the NS1A(1-73)−dsRNA Complex. Analysis of all the data presented here for the NS1A(1−73)−dsRNA complex reveals novel structural features which encode nonspecific dsRNA binding functions. The binding site of NS1A(1−73) consists of antiparallel helices 2 and 2′ with an Arg-rich surface. *A hypothetical model* that is consistent with our cumulative knowledge of the dsRNA binding properties of NS1A(1−73) features a symmetric structure with the binding surface of the protein spanning the minor groove of canonical A-form RNA (Figure 8). *We emphasize that this picture is just a working model, consistent with the available data.* In this *hypothetical model*, outward-directed arginine and lysine side chains of antiparallel helices 2 and 2′ interact in a symmetric fashion with the antiparallel

phosphate backbones that form the edges of the major groove. The strikingly similar spacing between the axes of helices 2 and 2′ of NS1A(1−73) (∼16.5 Å) and the interphosphate distance across the minor groove (∼16.8 Å) adds further credence to a model in which NS1A(1−73) "sits over" the minor groove of A-form RNA, and requires the A-form conformation for proper docking. Moreover, these protein−RNA interactions require little or no sequence specificity, also consistent with the lack of characterized sequence specificity in interactions of NS1A with dsRNA (*3*, *4*, *11*).

Comparison with Other Protein−dsRNA Complexes. When placed in the context of known RNA−protein interactions, our putative NS1A(1−73)−dsRNA model constitutes a novel mode of protein−dsRNA complex formation. Arginine-rich α-helical peptides, such as that derived from the HIV-1 Rev protein, are known to bind dsRNA through specific interactions in the major groove (*49*). However, the major groove in canonical A-form duplexes is too narrow and deep to accommodate even a single α-helix. As a result, in the Rev protein−RNA complex, binding of the Arg-rich helix results in severe distortions to the structure of the nucleic acid (*49*). Hence, an analogous interaction between helices 2 and 2′ of NS1A(1−73) and the major groove of its dsRNA target can be ruled out since both the protein and nucleic acid retain their free-state conformations upon complex formation.

The vast majority of dsRNA-binding proteins typically contain more than one copy of a ubiquitous ca. 70-amino acid, $\alpha_1-\beta_1-\beta_2-\beta_3-\alpha_2$ module called the dsRNA binding motif (dsRBD) (*50*). In the X-ray crystal structure of a dsRBD from *X. lae*vis RNA-binding protein A in complex with dsRNA (*19*), the two α-helices plus a loop between two of the strands form interactions collectively spanning a 16 bp window—two minor grooves and the intervening major groove—on one face of the duplex. The NMR structure of dsRBD3 from the *D. melanogaster* Staufen protein (*18*) again shows that the primary protein−RNA interactions involve the α-helices and loops (loop 2, between β1 and β2, and loop 4, between β3 and α2) from the protein and both the minor groove (with loop 2) and phosphodiester backbone (with loop 4 and α2) of the dsRNA. However, in this structure α1 interacts with a single-stranded stem loop capping the dsRNA helix. In both dsRBD−dsRNA complex structures, the protein−RNA interactions do not involve direct contact with the bases, indicative of sequence-independent complex formation. Moreover, as is the case for NS1A(1−73), the protein−nucleic acid interactions in both of these protein−dsRNA complexes involve only minor perturbations to the structures of both the protein and dsRNA upon complex formation. However, unlike our model, in these dsRBD−RNA complexes, nonhelical regions of the protein form critical contacts with the nucleic acid. In addition to including nonhelical conformations that are essential for nucleic acid recognition, which are not present in NS1A(1−73) and do not appear to form in NS1A(1−73) upon complex formation, these dsRBD modules lack the symmetry features of NS1A(1−73) which are probably exploited in the molecular recognition process.

Conclusions. This study demonstrates a system for studying interactions between the N-terminal RNA-binding domain of NS1A and a short 16 bp synthetic dsRNA. On the basis of gel filtration and sedimentation equilibrium measurements, the dimeric NS1A(1−73) domain binds to the dsRNA duplex with a 1:1 stoichiometry, yielding a complex with an apparent dissociation constant (K_d) of ∼1 μM. Circular dichroism and NMR data demonstrate little or no structural change of the protein or RNA upon complex formation, and that the dsRNA-binding epitope of NS1A-(1−73) includes residues of helices 2 and 2′. Analytical gel filtration and gel shift studies of the interaction between NS1A(1−73) and different double-stranded nucleic acids indicate that NS1A(1−73) recognizes canonical A-form dsRNA, but does not bind to dsDNA or dsRNA−DNA hybrids, which feature a B-type or A/B-type intermediate conformation, respectively. These studies provide a working model of the NS1A(1−73)−dsRNA complex, as well as the basis for designing several assays of NS1A(1−73)−dsRNA interactions that are useful in screening small molecules for candidate inhibitors of the association process. The complex described in this work is well-characterized, easily generated, and well-suited for detailed structural studies of the interactions underlying the NS1A−RNA molecular recognition process. Though the actual structure of the NS1A(1−73)−dsRNA complex remains to be elucidated, it is clear from the data presented in this paper that mode of binding dsRNA by NS1A(1−73) is distinct from that used by the dsRBD modules.

ACKNOWLEDGMENT

Y.X. thanks Dr. David Yphantis and Dr. Emory Braswell for helpful discussions.

REFERENCES

1. Wright, P. F., and Webster, R. G. (2001) Orthomyxoviruses, in *Fields Virology* (Knipe, D. M., and Howley, P. M., Eds.) 4th ed., pp 1533−1579, Lippincott Williams & Wilkins, Philadelphia.
2. Lamb, R. A., and Krug, R. M. (2001) Orthomyxoviridae: the viruses and their replication, in *Fields Virology* (Knipe, D. M., and Howley, P. M., Eds.) 4th ed., pp 1487−1532, Lippincott Williams & Wilkins, Philadelphia.
3. Hatada, E. R., and Fukuda, R. (1992) Binding of influenza A virus NS1 protein to dsRNA in vitro, *J. Gen. Virol. 73*, 3325−3329.
4. Lu, Y., Wambach, M., Katze, M. G., and Krug, R. M. (1995) Binding of the influenza virus NS1 protein to double-stranded RNA inhibits the activation of the protein kinase that phosphorylates the elF-2 translation initiation factor, *Virology 214*, 222−228.
5. Wang, W., and Krug, R. W. (1996) The RNA-binding and effector domains are conserved to different extents among influenza A and B viruses, *Virology 223*, 41−50.
6. Nemeroff, M., Barabino, S. M. L., Keller, W., and Krug, R. M. (1998) Influenza virus NS1 protein interacts with the 30 kD subunit of cleavage and specificity factor and inhibits 3′ end formation of cellular pre-mRNAs, *Mol. Cell 1*, 991−1000.
7. Chen, Z., Li, Y., and Krug, R. M. (1999) Influenza A virus NS1 protein targets poly(A)-binding protein II of the cellular 3′ end processing machinery, *EMBO J. 18*, 2273−2283.
8. Chen, C., and Krug, R. M. (2000) Selective nuclear export of viral mRNAs in influenza-virus-infected cells, *Trends Microbiol. 8*, 376−383.
9. Li, Y., Chen, Z. Y., Wang, W., Baker, C. C., and Krug, R. M. (2001) The 3′-end-processing factor CPSF is required for the splicing of single-intron pre-mRNAs in vivo, *RNA 7*, 920−931.
10. Qian, X.-Y., Alonso-Caplen, F., and Krug, R. M. (1994) Two functional domains of the influenza virus NS1 protein are required for regulation of nuclear export of mRNA, *J. Virol. 68*, 2433−2441.
11. Qian, X.-Y., Chien, C.-Y., Lu, Y., Montelione, G. T., and Krug, R. M. (1995) An amino-terminal polypeptide fragment of the influenza virus NS1 protein possesses specific RNA-binding activity and largely helical backbone structure, *RNA 1*, 948−956.

12. Chien, C.-Y., Tejero, R., Huang, Y., Zimmerman, D. E., Ríos, C. B., Krug, R. M., and Montelione, G. T. (1997) A novel RNA-binding motif in influenza A virus non-structural protein 1, *Nat. Struct. Biol. 4*, 891−895.
13. Liu, J., Lynch, P. A., Chien, C.-Y., Montelione, G. T., Krug, R. M., and Berman, H. M. (1997) Crystal structure of the unique RNA-binding domain of the influenza virus NS1 protein, *Nat. Struct. Biol. 4*, 896−899.
14. Wang, W., Riedel, K., Lynch, P., Chien, C.-Y., Montelione, G. T., and Krug, R. M. (1999) RNA binding by the novel helical domain of the influenza virus NS1 protein requires its dimer structure and a small number of specific basic amino acids, *RNA 5*, 195−205.
15. Nanduri, S., Carpick, B. W., Yang, Y., Williams, B. R., and Qin, J. (1998) Structure of the double-stranded RNA-binding domain of the protein kinase PKR reveals the molecular basis of its dsRNA-mediated activation, *EMBO J. 17*, 5458−5465.
16. Kharrat, A., Macias, M. J., Gibson, T. J., Nilges, M., and Pastore, A. (1995) Structure of the dsRNA binding domain of *E. coli* RNase III, *EMBO J. 14*, 3572−3584.
17. Bycroft, M., Grunert, S., Murzin, A. G., Proctor, M., and St. Johnston, D. (1995) NMR solution structure of a dsRNA binding domain from *Drosophila* Staufen protein reveals homology to the N-terminal domain of ribosomal protein S5, *EMBO J. 14*, 3563−3571.
18. Ramos, A., Grunert, S., Adams, J., Micklem, D. R., Proctor, M. R., Freund, S., Bycroft, M., St. Johnston, D., and Varani, G. (2000) RNA recognition by a Staufen double-stranded RNA-binding protein, *EMBO J. 19*, 997−1009.
19. Ryter, J. M., and Schultz, S. C. (1998) Molecular basis of double-stranded RNA-protein interactions: structure of a dsRNA-binding domain complexed with dsRNA, *EMBO J. 17*, 7505−7513.
20. Qiu, Y., Nemeroff, M. E., and Krug, R. M. (1995) The influenza virus NS1 protein binds to a specific region in human U6 snRNA and inhibits U6−U2 and U6−U4 snRNA interactions during splicing, *RNA 1*, 304−316.
21. Jansson, M., Li, Y.-C., Jendeberg, L., Anderson, S., Montelione, G. T., and Nilsson, B. (1996) High-level production of uniformly ^{15}N- and ^{13}C-enriched fusion proteins in *Escherichia coli*, *J. Biomol. NMR 7*, 131−141.
22. Wincott, F., DiRenzo, A., Shaffer, C., Grimm, S., Tracz, D., Workman, C., Sweedler, D., Gonzalez, C., Scaringe, S., and Usman, N. (1995) Synthesis, deprotection, analysis and purification of RNA and ribozymes, *Nucleic Acids Res. 23*, 2677−2684.
23. Cantor, C. R., and Tinoco, I., Jr. (1965) Absorption and optical rotatory dispersion of seven trinucleoside diphosphates, *J. Mol. Biol. 13*, 65−77.
24. Johnson, M. L., Correia, J. J., Yphantis, D. A., and Halvorson, H. R. (1981) Analysis of data from the analytical ultracentrifuge by nonlinear least-squares techniques, *Biophys. J. 36*, 575−583.
25. Laue, T. M., Shah, B. D., Ridgeway, T. M., and Pelletier, S. L. (1992) Computer-aided interpretation of analytical sedimentation data for proteins, in *Analytical Ultracentrifugation in Biochemistry and Polymer Science* (Harding, S. E., Rowe, A. J., and Horton, J. C., Eds.) pp 90−125, Royal Society of Chemistry, Cambridge, U.K.
26. Cohn, E. J., and Edsall, J. T. (1943) Density and apparent specific volume of proteins, in *Proteins, Amino Acids and Peptides as Ions and Dipolar Ions* (Cohn, E. J., and Edsall, J. T., Eds.) pp 370−381, Rheinhold, New York.
27. Yphantis, D. A., and Waugh, D. F. (1956) Ultracentrifugal characterization by direct measurement of activity. I. Theoretical, *J. Phys. Chem. 60*, 623−629.
28. Van Holde, K. E., and Baldwin, R. L. (1958) Rapid attainment of sedimentation equilibrium, *J. Phys. Chem. 62*, 734−743.
29. Zimmerman, D. E., Kulikowski, C. A., Huang, Y., Feng, W., Tashiro, M., Shimotakahara, S., Chien, C.-Y., Powers, R., and Montelione, G. T. (1997) Automated analysis of protein NMR assignments using methods from artificial intelligence, *J. Mol. Biol. 269*, 592−610.
30. Wishart, D. S., Bigam, C. G., Yao, J., Abildgaard, F., Dyson, J., Oldfield, E., Markley, J. L., and Sykes, B. D. (1995) ^{1}H, ^{13}C and ^{15}N chemical shift referencing in biomolecular NMR, *J. Biomol. NMR 6*, 135−140.
31. Montelione, G. T., Ríos, C. B., Swapna, G. V. T., and Zimmerman, D. E. (1999) NMR pulse sequences and computational approaches for automated analysis of sequence-specific backbone assignments of proteins, in *Biological Magnetic Resonance: Structure Computation and Dynamics in Protein NMR* (Berliner, L. J., and Krishna, N. R., Eds.) Vol. 17, pp 81−130, Kluwer Academic/Plenum Publishers, New York.
32. Roberts, R. W., and Crothers, D. M. (1992) Stability and properties of double and triple helices: dramatic effects of RNA or DNA backbone composition, *Science 258*, 1463−1466.
33. Ratmeyer, L., Vinayak, R., Zhong, Y. Y., Zon, G., and Wilson, W. D. (1994) Sequence specific thermodynamic and structural properties for DNA·RNA duplexes, *Biochemistry 33*, 5298−5304.
34. Lesnik, E. A., and Freier, S. M. (1995) Relative thermodynamic stability of DNA, RNA, and DNA:RNA hybrid duplexes: relationship with base composition and structure, *Biochemistry 34*, 10807−10815.
35. Ralston, G. (1993) in *Introduction to Analytical Ultracentrifugation*, Beckman Instruments, Inc.
36. Johnson, W. C., Jr. (1990) Protein secondary structure and circular dichroism: a practical guide, *Proteins 7*, 205−214.
37. Gray, D. M. (1996) *Circular Dichroism and the Conformational Analysis of Biomolecules*, pp 469−501, Plenum Press, New York.
38. Wells, B. D., and Yang, J. T. (1974) A computer probe of the circular dichroic bands of nucleic acids in the ultraviolet region. II. Double-stranded ribonucleic acid and deoxyribonucleic acid, *Biochemistry 13*, 1317−1321.
39. Gray, D. M., and Ratliff, R. L. (1975) Circular dichroism spectra of poly[d(AC):d(GT)], poly[r(AC):r(GU)], and hybrids poly-[d(AC):r(GU)] and poly[r(AC):d(GT)] in the presence of ethanol, *Biopolymers 14*, 487−498.
40. Gray, D. M., Morgan, A. R., and Ratliff, R. R. (1978) A comparison of the circular dichroism spectra of synthetic DNA sequences of the homopurine·homopyrimidine and mixed purine-pyrimidine types, *Nucleic Acids Res. 5*, 3679−3695.
41. Gray, D. M., Ratliff, R. L., and Vaughan, M. R. (1992) Circular dichroism spectroscopy of DNA, *Methods Enzymol. 211*, 389−406.
42. Hung, S.-H., Yu, Q., Gray, D. M., and Ratliff, R. L. (1994) Evidence from CD spectra that d(purine)·r(pyrimidine) and r(purine)·d(pyrimidine) hybrids are in different structural classes, *Nucleic Acids Res. 22*, 4326−4334.
43. Clark, C. L., Cecil, P. K., Singh, D., and Gray, D. M. (1997) CD, absorption and thermodynamic analysis of repeating dinucleotide DNA, RNA and hybrid duplexes $[d/r(AC)]_{12}$·$[d/r(GT/U)]_{12}$ and the influence of phosphorothioate substitution, *Nucleic Acids Res. 25*, 4098−4105.
44. Dickerson, R. E., Drew, H. R., Conner, B. N., Wing, R. M., Fratini, A. V., and Kopka, M. L. (1982) The anatomy of A-, B-, and Z-DNA, *Science 216*, 475−485.
45. Arnott, S., Fuller, W., Hodgson, A., and Prutton, I. (1968) Molecular conformations and structure transitions of RNA complementary helices and their possible biological significance, *Nature 220*, 561−564.
46. Egli, M., Usman, N., and Rich, A. (1993) Conformational influence of the ribose 2′-hydroxyl group: crystal structures of DNA-RNA chimeric duplexes, *Biochemistry 32*, 3221−3237.
47. Gyi, J. I., Conn, G. L., Lane, A. N., and Brown, T. (1996) Comparison of the thermodynamic stabilities and solution conformations of DNA·RNA hybrids containing purine-rich and pyrimidine-rich strands with DNA and RNA duplexes, *Biochemistry 35*, 12538−12548.
48. Benevides, J. M., Wang, A. H., Rich, A., Kyogoku, Y., van der Marel, G. A., van Boom, J. H., and Thomas, G. J., Jr. (1986) Raman spectra of single crystals of r(GCG)d(CGC) and d(CCCCGGGG) as models for A DNA, their structure transitions in aqueous solution and comparison with double-helical poly(dG)·poly(dC), *Biochemistry 25*, 41−50.
49. Battiste, J. L., Mao, H., Rao, N. S., Tan, R., Muhandiram, D. R., Kay, L. E., Frankel, A. D., and Williamson, J. R. (1996) Alpha helix-RNA major groove recognition in an HIV-1 rev peptide-RRE RNA complex, *Science 273*, 1547−1551.
50. Fierro-Monti, I., and Matthews, M. B. (2000) Proteins binding to duplexed RNA: one motif, multiple functions, *Trends Biochem. Sci. 25*, 241−246.

BI030176O